Electronic and optical properties of HgI_2

Yia-Chung Chang
Department of Physics, University of Illinois at Urbana-Champaign, 1110 West Green Street, Urbana, Illinois 61801 and Materials Research Laboratory, University of Illinois at Urbana-Champaign, 1110 West Green Street, Urbana, Illinois 61801

R. B. James
Advanced Material Research Division, Sandia National Laboratories, Livermore, California 94550
(Received 28 February 1992)

Empirical nonlocal pseudopotential calculations of the electronic band structure of undoped mercuric iodide in its red tetragonal form are presented. Values for the electron and hole effective masses, optical matrix elements for interband transitions, and complex dielectric function are reported. Excitonic effects on the absorption coefficient near the fundamental band gap are included within the effective-mass approximation. The resulting absorption spectra and the polarization dependence are in good agreement with experiment. The dielectric-function spectra for photon energies between 2 and 10 eV are also calculated and they are in fair agreement with available data.

I. INTRODUCTION

Mercuric iodide (HgI_2) in its red tetragonal form has many properties that make it well suited for use as a γ- and x-ray spectrometer that can be operated at room temperature.[1-5] These properties include relatively large atomic masses (i.e., $Z = 80$ and 53 for Hg and I, respectively) which allows for a high stopping power to energetic photons, a high bulk resistivity ($\approx 1013\ \Omega\,\mathrm{cm}$) (Ref. 6) which ensures a low dark current during detector operation, and a high photosensitivity so that the number of photogenerated electron-hole pairs is proportional to the energy of the incident photon. Although the potential of HgI_2 for fabricating high-resolution x-ray and γ-ray spectrometers has been well demonstrated,[7] there continues to be significant problems associated with carrier trapping, in which case the amount of charge collected is not a unique function of the γ- or x-ray energy. These transport problems have motivated considerable research in the optical and electrical properties of HgI_2, particularly those properties that might be related to detector performances.[8-24]

There have been numerous experimental reports on the optical properties of HgI_2.[8-11,16,17] However, theoretical investigations on this subject are still lacking. One difficulty frequently encountered in interpreting the optical and electrical measurements is the lack of knowledge of the electronic band structure of the material. Yee, Sherohman, and Armantrout reported the first empirical pseudopotential calculation on HgI_2.[25] Unfortunately, the crystal structure used in their calculations is incorrect; thus, their results bear little relation with reality. Turner and Harmon[26] reported the first self-consistent calculation within the local-density approximation. They also included the relativistic effect and the spin-orbit interaction. The overall band structures obtained by this method are quite reliable, except that the fundamental band gap is too small due to the local-density approximation. As a result, the effective masses predicted by this calculation are also too small. In this paper, we report an empirical nonlocal pseudopotential calculation of the electronic and optical properties of HgI_2, including the effects of the spin-orbit interaction. Values for the effective masses and real and imaginary part of the complex dielectic function are also presented.

II. METHOD

The method used here is basically the same as that described in Ref. 27. The local pseudopotentials of the mercury and iodine are taken to have the form introduced in Ref. 28. Namely,

$$V_L(\mathbf{q}) = a_1(q^2 - a_2)/(e^{a_3(q^2-a_4)} + 1). \quad (1)$$

The parameters a_2, a_3, and a_4 for I are taken to be the same as given in Ref. 28, and those for Hg are determined by fitting the screened atomic pseudopotential given in Ref. 29. These parameters for both Hg and I are tabulated in Table I. The parameter a_1 which determines the strength of the pseudopotential is treated as an empirical parameter. The nonlocal pseudopotentials are taken to have the form given in Ref. 27,

TABLE I. Empirical parameters for Hg and I local pseudopotentials defined in Eq. (1). The units of distances are in Bohrs and the energy units are in Rydbergs.

	a_1	a_2	a_3	a_4
Hg	0.35	1.4	0.55	−2.5
I	5.294	1.7	0.46	−6.5

$$V_{\rm NL}(\mathbf{k},\mathbf{G}-\mathbf{G}')$$

$$= 4\pi \sum_l (2l+1) P_l(\cos\theta) \times \int dr\, r^2 V_l(r) j_l(Kr) j_l(K'r)/\Omega_a, \qquad (2)$$

where $\mathbf{K}=\mathbf{k}+\mathbf{G}$, $\cos\theta = \mathbf{K}\cdot\mathbf{K}'/KK'$, Ω_a is the atomic volume, P_l is a Legendre polynomial, j_l is a spherical Bessel function, and $V_l(r) = A_l e^{-(r/R)^2}$. We use $R = 2.3a_B$, where a_B is the Bohr radius. A_l is an adjustable parameter for each value of l. Since the states of interest are either s-like or p-like, we only keep $l=0$ and 1. In order to fit the energy spacing between the heavy-hole and light-hole states due to the tetragonal crystal field, we introduce an anisotropy factor μ, which modifies the spherical local pseudopotential to describe a tetragonal one, i.e.,

$$V_L(q_x,q_y,q_z) \rightarrow V_L(q_x,q_y,\mu q_z).$$

Thus we have seven empirical parameters: a_1, A_0, A_1 for both Hg and I plus the anisotropy factor μ. These parameters are adjusted to fit the band gap to the experimental value (2.37 eV) (Ref. 8) and the overall band structure to the results obtained by a first-principles calculation.[26] The optimized parameters are listed in Tables I and II. In our calculations, approximately 620 plane waves with energies less than E_1 (=8 Ry) are included in the diagonalization procedure. Here Ry denotes a rydberg.

The unit cell consists of two Hg atoms and four I atoms (see Ref. 26). The solid has inversion symmetry about the midpoint between the two Hg atoms in a unit cell. If we choose the point as the origin of the coordinate system, the atomic positions of the two Hg atoms are $(-a/4,-a/4,-c/4)$ and $(a/4,a/4,c/4)$, and those of the four I atoms are $(-a/4,a/4,-0.111c)$, $(a/4,-a/4,0.111c)$, $(-a/4,a/4,0.389c)$, and $(a/4,-a/4,-0.389c)$. Here, $a=b=4.37$ Å and $c=12.44$ Å. With the inversion symmetry, the Hamiltonian matrix elements between any two plane waves are real, and the eigenvalue problem can be solved efficiently.

When the spin-orbit interaction is included, the Hamiltonian matrix becomes complex and its dimension is doubled. This makes the direct diagonalization very time consuming. We thus elect to include the spin-orbit-interaction effects by first-order degenerate perturbation theory. We first evaluate the matrix elements of the spin-orbit term using the zero-order eigenstates of the lowest-lying 30 bands (or 60 bands including the spin degeneracy). We then diagonalize the 60 × 60 complex matrix to obtain the energy eigenvalues which include the effect of spin-orbit interaction. The matrix elements of the spin-orbit term for p-like states are given by[28,30]

$$\langle \mathbf{K},s|H_{\rm so}|\mathbf{K}',s'\rangle = -i\sum_j \lambda_j S_j(\mathbf{K}-\mathbf{K}')\sigma_{ss'}\cdot(\mathbf{K}\times\mathbf{K}'),$$

where the subscript j denotes the atomic species (Hg or I), S_j is the structure factor, $\sigma_{ss'}$ are elements of the Pauli matrices between two spin states s and s', and λ_j is the atomic spin-orbit coupling parameter, which is adjusted to give the correct spin-orbit splitting at the zone center. We found that the most appropriate value for λ is 0.023 (in units of Rya_B^2).

The imaginary part of the dielectric function (ϵ_2) is given by[31]

$$\epsilon_2(\omega) = \frac{4\pi^2e^2}{m^2V\omega^2}\sum_{\mathbf{k},ij} |\langle \mathbf{k},i|\hat{e}\cdot\mathbf{p}|\mathbf{k},j\rangle|^2 \times \delta[E_j(\mathbf{k})-E_i(\mathbf{k})-\hbar\omega], \qquad (3)$$

where $|\mathbf{k},i\rangle$ denotes the ith electronic state of the solid associated with wave vector $\mathbf{k}$, $\hat{e}$ is the polarization vector, $\mathbf{p}$ is the momentum operator, and V is the volume of the solid. To perform the sum in Eq. (3), we used 75 special points in the irreducible $\frac{1}{16}$ section of the first Brillouin zone, and the δ function was replaced by a Lorentzian function with half-width of 0.1 eV to account for lifetime broadening of the electrons and holes.

TABLE II. Empirical parameters for Hg and I nonlocal pseudopotentials defined in Eq. (2) and the anisotropy factor squared, μ^2. All energy parameters are in units of Rydbergs.

	A_0	A_1	μ^2
Hg	−0.575	0.0	1.06
I	−0.9	−0.4	1.06

III. RESULTS

Figure 1 shows the calculated band structure of HgI_2 without including the spin-orbit interaction. The band structure has been rigidly shifted by a constant so that the energy of the valence-band maximum is zero after inclusion of the spin-orbit interaction effects. Since the space group of the crystal is D_{4h}, the states with x- and y-like symmetry are degenerate at the zone center, whereas states with s-like and z-like symmetry are nondegenerate. Throughout the paper, we have chosen the z direction to be parallel to the c axis of the crystal. In Fig. 1 we see

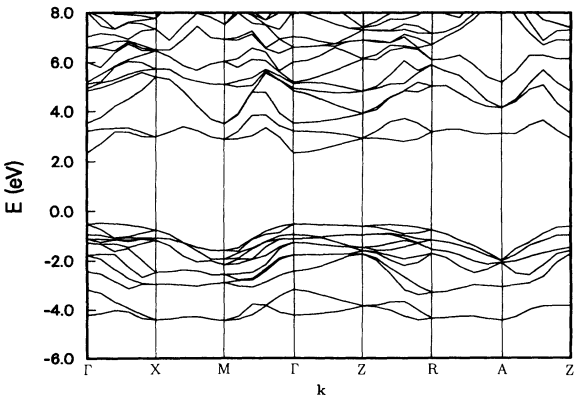

FIG. 1. Band structures of HgI_2 without spin-orbit interaction.

four pairs of doubly degenerate levels at the zone center with energies between −2 and 0 eV. They correspond to the I $5p_x$ and $5p_y$ nonbonding states (see Ref. 26). The two nondegenerate levels near −1.5 and −2.5 eV correspond to the I $5p_z$ nonbonding states. The two remaining I $5p_z$ orbitals interact with the two Hg $6s$ orbitals to form two bonding states with energies between −4.5 and −3 eV and two antibonding states with energies between 2.3 and 3.5 eV. The I $5s$ levels are near −11 eV (not shown). The Hg $6p$ and I $5d$ levels are distributed from 3.5 to 10 eV, among which the doubly degenerate ones can be identified as the Hg p_x and p_y states. Note that the Hg $5d$ levels, which are between the I $5s$ and Hg $6s$–I $5p_z$ bonding states, are considered as core levels in the present pseudopotential model. Hence, they will not show up in the band structure.

Figure 2 shows the calculated band structure of HgI_2 with the spin-orbit interaction. All bands are rigidly shifted by a constant so that the valence-band maximum is at zero. The main difference between this figure and Fig. 1 is that the doubly degenerate levels at zone center in Fig. 1 are now split by the spin-orbit interaction with a splitting of ≈ 0.7 eV. With the adjusted parameters listed in Tables I and II, the fundamental band gap becomes 2.37 eV and the splitting between the first two valence bands (i.e., heavy-hole and light-hole bands) is 0.2 eV, which both agree with the measured values at 4.2 K.[8,9] The overall band structures are also in qualitative agreement with those obtained by Turner and Harmon.[26]

Figure 3 shows the closeup view of the band structures of HgI_2 near the zone center. In the left part the wave vector $\mathbf{k}$ is along the [110] direction, and in the right part it is along the [001] direction. The unit of k is in $2\pi/a$. We have found that the conduction band is nearly isotropic, whereas the valence band is more anisotropic. The effective masses deduced from this plot are shown in Table III, together with the experimental values. The agreement between theory and experiment is fairly good. The polaron masses (m^e and m^h) are obtained by an intermediate-coupling polaron theory with the use of LO-phonon energies and high-freqency and low-frequency anisotropic dielectric constants as provided in Ref. 11. The theory predicts that $m_{e,\parallel} > m_{e,\perp}$, while the cyclotron-resonance measurements found the opposite. On the other hand, the values deduced from optical measurements[17] seem to support our prediction.

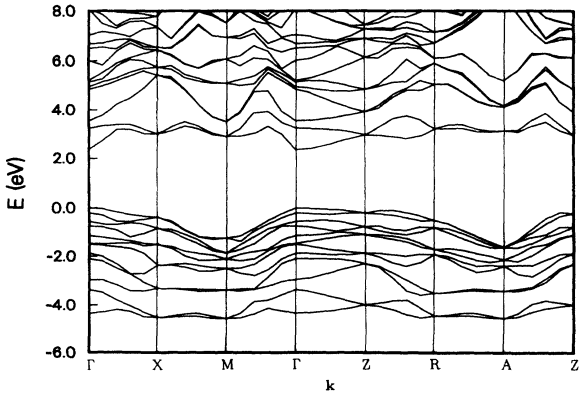

FIG. 2. Band structures of HgI_2 with spin-orbit interaction.

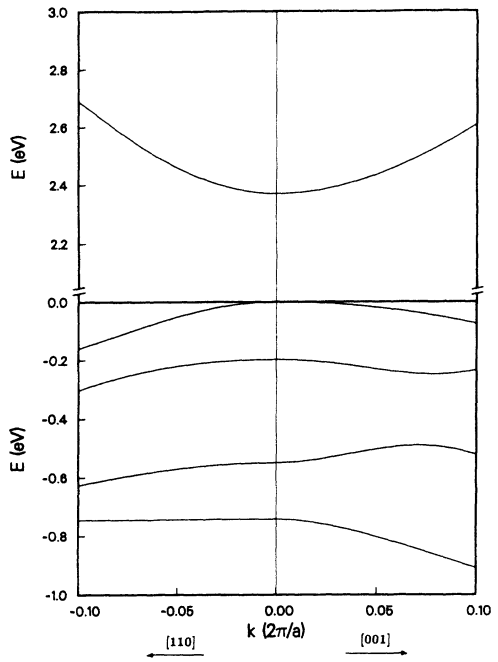

FIG. 3. Band structures of HgI_2 near the zone center.

Figure 4 shows the squared optical matrix elements P^2 for interband transitions involving the topmost five valence bands and the lowest conduction band near the zone center. Here P^2 is defined as

$$P_{ij}^2 = \frac{2}{m}|\langle \mathbf{k}, i|\hat{e}\cdot\mathbf{p}|\mathbf{k}, j\rangle|^2. \tag{4}$$

The solid curves are for the in-plane polarization ($\hat{e} \perp \hat{z}$) and the dashed curves are for polarization along the c axis ($\hat{e}\|\hat{z}$). The labels $v1, ..., v5$ denote the first to fifth valence band. We see that for the $v1$ curve, the z-polarization component is very weak for all values of $\mathbf{k}$ and vanishes at the zone center. This is consistent with the heavy-hole character, since the heavy-hole state transforms like $(x+iy)\uparrow$. Here $\uparrow$ denotes an up spin. For the $v2$ curve, the z component is strong and the x (or y) component is about $\frac{1}{6}$ of that for the $v1$ curve. This is consistent with the nature of the light-hole state, since the light-hole state is the linear combination of states transforming like $(x+iy)\downarrow$ and $z\uparrow$ with a majority component in $z\uparrow$. It should be noted that the optical matrix elements calculated by using the pseudo-wave-functions are not precise, because the corrections due to orthogonalization to the core electronic states are not included. The size of the correction is difficult to estimate. However, based on a comparison between the experimental value and the calculated value within the pseudopotential method for

TABLE III. Effective masses for motion perpendicular to ($m_\perp$) and parallel to the c axis ($m_\parallel$). The subscripts and superscripts e and h denote electron and hole, respectively. The subscripts apply to the bare effective masses and the superscript apply to the polaron effective masses.

	$m_{e,\perp}$	$m_{e,\parallel}$	$m_\perp^e$	$m_\parallel^e$	$m_{h,\perp}$	$m_{h,\parallel}$	$m_\perp^h$	$m_\parallel^h$	$\mu_\perp$	$\mu_\parallel$
Theory	0.22	0.30	0.29	0.37	0.59	1.02	0.89	1.43	0.22	0.29
Experiment	0.29[a]	0.25[a]	0.37[a]	0.31[a]	0.56[a]	1.72[a]	1.03[a]	2.06[a]	0.24[b]	0.31[b]

[a]Reference 28.
[b]Reference 17.

typical semiconductors (see Ref. 31), the error in optical responses is about 10–20%.

Knowing the optical matrix elements and effective masses near the zone center, we can model the absorption coefficient near the fundamental band gap, including the excitonic effect. This is done within the effective-mass approximation. The effective-mass Hamiltonian for the exciton in an anisotropic medium is

$$H_{ex} = -\frac{1}{2\mu_\perp}(\partial_x^2 + \partial_y^2) - \frac{1}{2\mu_\parallel}\partial_z^2 - \frac{e^2}{\epsilon_a r}, \tag{5}$$

where $\mathbf{r}$ is the electron-hole relative coordinate, ϵ_a is some average dielectric constant, which will be determined later, and $\mu_\perp$ and $\mu_\parallel$ are the in-plane and c-axis reduced effective masses, respectively. They are related to the corresponding electron and hole polaron masses via

$$\frac{1}{\mu_{\perp,\parallel}} = \frac{1}{m^e_{\perp,\parallel}} + \frac{1}{m^h_{\perp,\parallel}}.$$

The predicted reduced polaron masses are also shown in Table III.

The eigenstates for an anisotropic Hamiltonian can be solved by numerical methods.[32] However, for our purposes here, it suffices to use a spherical approximation in which the anisotropic reduced mass is replaced by a spherically averaged reduced mass given by[33]

$$\frac{1}{\mu_a} = \left(\frac{2}{\mu_\perp} + \frac{1}{\mu_\parallel}\right)\Big/3.$$

In this approximation, the exciton binding energy is given by $E_X = (\mu_a/m_0\epsilon_a^2)13.6$ eV. We choose a value for ϵ_a such that E_X is equal to the experimental value of 0.032 eV.[17] We found that $\epsilon_a \approx 10.1$, which is between the average low-frequency and high-frequency dielectric constants.[11] In the spherical effective-mass theory, the absorption coefficient for each pair of conduction and valence bands is given by[31]

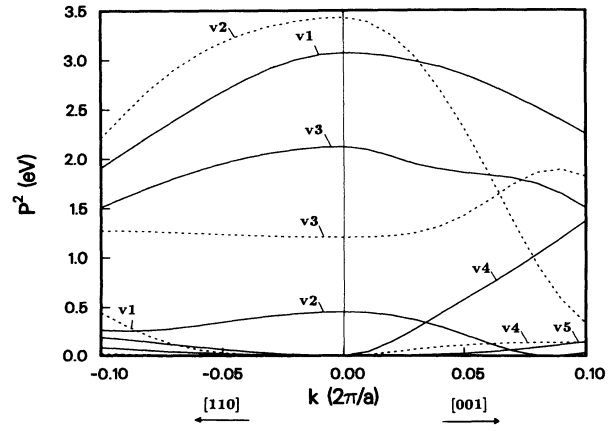

FIG. 4. Optical matrix elements near the zone center for interband transitions.

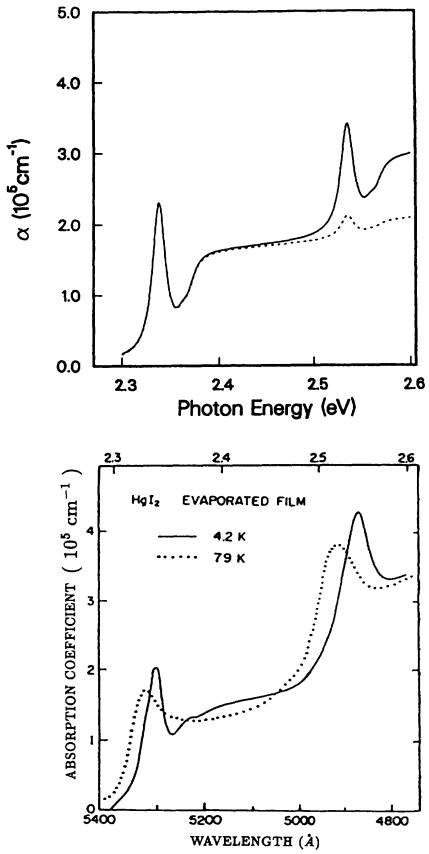

FIG. 5. Absorption spectra of HgI_2 near the fundamental absorption edge. Top: theoretical prediction; the solid curve is for unpolarized light and the dashed curve is for light polarized perpendicular to the c axis. Bottom: data from Ref. 26; both curves are for unpolarized light.

$$\alpha(\omega) = \frac{4\pi^2 e^2}{mcnV\omega} \times P^2 \left[(2m/\hbar^2)^{3/2} \pi E_X e^u / \sinh u + \sum_n |\phi_n(\mathbf{0})|^2 \delta(\hbar\omega - E_g + E_X/n^2) \right], \quad (6)$$

where P^2 is the squared optical matrix element defined in Eq. (4) and evaluated at the zone center, $u = \pi[E_X/(\hbar\omega - E_g)]^{1/2}$, E_g denotes the band gap, n denotes the principal quantum number for the exciton bound states, and $\phi_n(\mathbf{0})$ is the exciton envelope function evaluated at the origin for the nth bound state. Using Eq. (6) and including the $n = 1$ and 2 exciton bound states, we obtain an absorption spectrum for HgI_2 near the fundamental gap as shown in Fig. 5. Both the transitions from the heavy-hole and light-hole bands to the lowest conduction band are included. The binding energies of the heavy-hole and light-hole excitons are both taken to be 0.032 eV.[6] The solid curve shows the absorption spectrum for an unpolarized light, and the dashed curve shows the contribution due to the in-plane polarization alone (i.e., $\frac{2}{3}\alpha_\perp$, where $\alpha_\perp$ is the absorption coefficient for a linearly polarized light with $\hat{e} \perp \hat{z}$). Note that here

$$\alpha = (2\alpha_\perp + \alpha_\parallel)/3,$$

where $\alpha_\parallel$ is the absorption coefficient for a linearly polarized light with $\hat{e} \| \hat{z}$. The broadening parameter used is 0.008 eV. In Fig. 5 we have also included for comparison the experimental absorption coefficient for unpolarized light from Ref. 9. The calculated spectrum for the heavy-hole exciton agrees very well with experiment, while for the light-hole exciton, the calculated spectrum is about a factor of 2 too low compared to the experiment. We notice that the heavy-hole exciton absorption is nonzero only for light polarized perpendicular to the c axis, while the light-hole exciton absorption is nonzero for both polarizations with $\alpha_\parallel$ much stronger than $\alpha_\perp$. This is in qualitative agreement with the reflectivity measurement.[9]

Figure 6 shows the calculated dielectric-function spectra of HgI_2. The solid (dashed) curve is for polarization perpendicular (parallel) to the c axis. The ϵ_2 spectrum shows two major structures, centered around 4 and 7 eV, respectively. This is in qualitative agreement with the experimental results.[10] However, the height of the first structure is about a factor of 2 too small compared to data, whereas the integrated strength of the second strucure is too high. The calculated results shown here did not include the excitonic and local-field effects, which tend to enhance the lower-energy structure and reduce the higher-energy structure. These effects can be included approximately and empirically by using a "contact" excitonic potential with adjustable strength.[34] The corrected dielectric function ($\tilde{\epsilon}$) (i.e., including the exciton and local-field effects) is related to the "bare" dielectric function by[34,35]

$$\tilde{\epsilon}(\omega) - 1 = \frac{\epsilon(\omega) - 1}{1 - g_0\hbar^2\omega^2[\epsilon(\omega) - 1]}.$$

Here g_0 is an empirical parameter.

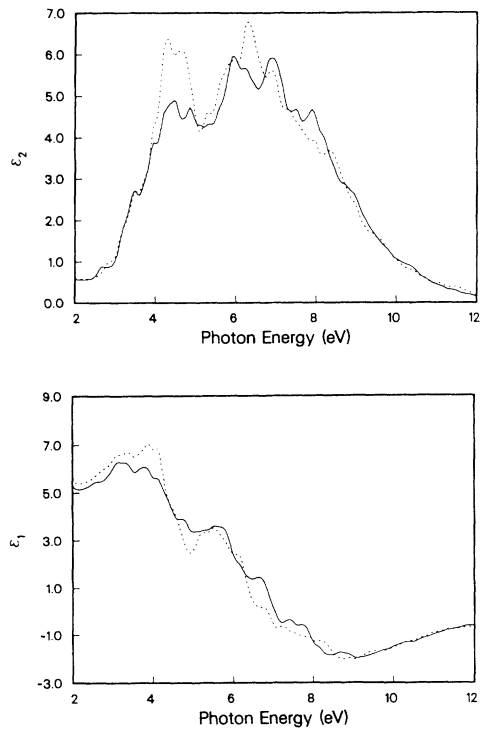

FIG. 6. Dielectric functions of HgI_2. Solid: $\hat{e} \perp \hat{z}$. Dotted: $\hat{e} \| \hat{z}$. Top: imaginary part. Bottom: real part.

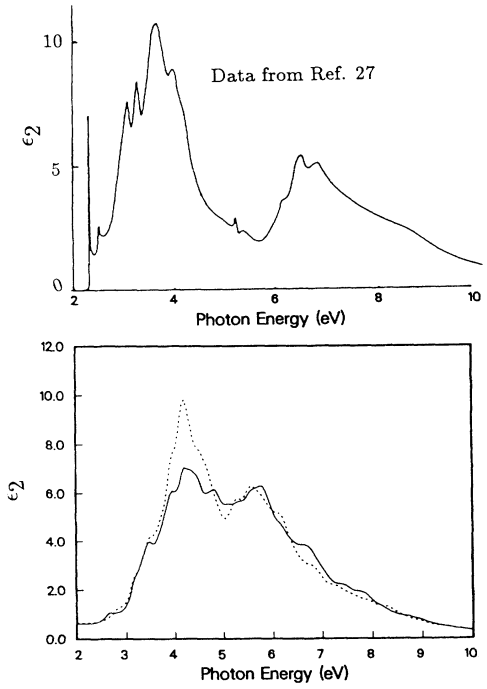

FIG. 7. Comparison of the imaginary part of the dielectric functions of HgI_2 between theory (bottom) and experiment (top). Data are taken from Ref. 27. For the bottom two curves, solid is for $\hat{e} \perp \hat{z}$ and dotted is for $\hat{e} \| \hat{z}$.

We found that with $g_0 \approx 0.003$ eV^{-2}, the corrected dielectric function is in better agreement with the experiment. This is shown in Fig. 7, in which we also include the experimental results obtained by Anedda *et al.* (Ref. 10). However, after including the exciton effects, the second structure becomes peaked at 6 eV, which is about 1 eV lower than the experimental value. The first structure is still too low compared to data, but the integrated strength is roughly correct. The real part of the dielectric constant is also slightly enhanced near the fundamental band gap. We get $\epsilon_\perp \approx 5.4$ and $\epsilon_\parallel \approx 5.8$ near the band gap, wheras the experimental values are $\epsilon_\perp \approx 5.15$ and $\epsilon_\parallel \approx 6.8$.[11]

IV. SUMMARY AND CONCLUSIONS

We have performed empirical nonlocal pseudopotential calculations on the electronic and optical properties of HgI_2, including the spin-orbit interaction. Both the conduction-band minimum and valence-band maximum are found to occur at the zone center. The conduction band is nearly isotropic, whereas the valence band is much more anisotropic. The curvatures of the bands near the zone center are used to calculate electron and hole effective masses, and comparisons with experiment are noted. Calculated values for the absorption coefficient and real and imaginary parts of the dielectric function are also presented.

ACKNOWLEDGMENTS

We acknowlege fruitful discussions with C. Y. Fong. We also thank D. N. Harmon for sending us some unpublished results, which have helped us greatly.

[1]W. R. Willig, Nucl. Instrum. Methods **96**, 615 (1971).
[2]J. P. Ponpon, R. Stuck, P. Siffert, B. Meyer, and C. Schwab, IEEE Trans. Nucl. Sci. **NS-22**, 182 (1975).
[3]A. J. Dabrowski, W. M. Szymczyk, J. S. Iwanczyk, J. H. Kusmiss, W. Drummond, and L. Ames, Nucl. Instrum. Methods **213**, 89 (1983).
[4]S. P. Swierkowski, G. A. Armantrout, and R. Wichne, IEEE Trans. Nucl. Sci. **NS-21**, 302 (1974).
[5]J. H. Howes and J. Watling, in *Nuclear Radiation Detector Materials*, edited by E. E. Haller, H. W. Kramer, and W. A. Higinbotham, MRS Symposia Proceedings No. 16 (Materials Research Society, Pittsburgh, 1983), p. 207.
[6]H. L. Malm, T. W. Raudoff, M. Martina, and K. R. Zanio, IEEE Trans. Nucl. Sci. **NS-20**, 500 (1973).
[7]See, for example, the review by R. C. Whited and M. Schieber, Nucl. Instrum. Methods **162**, 119 (1979).
[8]B. V. Novikov and M. M. Pimonenko, Fiz. Tekh. Poluprovodn. **4**, 2077 (1970) [Sov. Phys. Semicond. **4**, 1785 (1970)].
[9]K. Kanzaki and I. Imai, J. Soc. Jpn. **32**, 1003 (1972).
[10]A. Anedda, F. Raga, E. Grilli, and M. Guzzi, Nuovo Cimento **38**, 439 (1977).
[11]P. D. Bloch, J. W. Hodby, C. Schwab, and D. W. Stacey, J. Phys. C **11**, 2579 (1978).
[12]C. Dlasi, S. Galassini, C. Manfredotti, G. Micocci, L. Ruggiero, and A. Tepore, Nucl. Instrum. Methods **150**, 103 (1978).
[13]U. Gelbert, Y. Yacoby, I. beinglass, and A. Holzer, IEEE Trans. Nucl. Sci. **NS-24**, 135 (1977).
[14]J. C. Muller, A. Friant, and P. Siffert, Nucl. Instrum. Methods **150**, 97, (1978).
[15]M. Schieber, I. Beinglass, G. Dishon, A. Holzer, and G. Yaron, Nucl. Instrum. Methods **150**, 71 (1978).
[16]A. Anedda, E. Grilli, M. Guzzi, F. Raga, and A. Serpi, Solid State Commun. **39**, 1121 (1981).
[17]T. Goto and A. Kasuya, J. Soc. Jpn. **50**, 520 (1981).
[18]S. R. Kurtz, R. C. Hughes, C. Ortale, and W. F. Schnepple, J. Appl. Phys. **62**, 4308 (1987).
[19]D. Wong, X. J. Bao, T. E. Schlesinger, R. B. James, A. Cheng, C. Ortale, and L. van den Berg, Appl. Phys. Lett. **53**, 1536 (1988).
[20]R. B. James, X. J. Bao, T. E. Schlesinger, J. M. Markakis, A. Y. Cheng, and C. Ortale, J. Appl. Phys. **66**, 2578 (1989).
[21]R. B. James, X. J. Bao, T. E. Schlesinger, C. Ortale, and L. van den Berg, J. Appl. Phys. **67**, 2571 (1990).
[22]X. J. Bao, T. E. Schlesinger, R. B. James, R. H. Stulen, C. Ortale, and L. van den Berg, J. Appl. Phys. **68**, 86 (1990).
[23]L. R. Williams, R. J. M. Anderson, and M. J. Banet, Chem. Phys. Lett. **182**, 422 (1991).
[24]X. J. Bao, T. E. Schlesinger, R. B. James, G. L. Gentry, A. Y. Cheng, and C. Ortale, J. Appl. Phys. **69**, 4247 (1991).
[25]J. H. Yee, J. W. Sherohman, and G. A. Armantrout, IEEE Trans. Nucl. Sci. **NS-23**, 117 (1976).
[26]D.E. Turner and B. N. Harmon, Phys. Rev. B **40**, 10516 (1989).
[27]J. R. Chelikowsky and M. L. Cohen, Phys. Rev. B **14**, 556 (1976).
[28]I. Ch. Schluter and M. Schluter, Phys. Rev. B **9**, 1652 (1974).
[29]G. B. Brandt and J. A. Rayne, Phys. Rev. **148**, 644 (1966).
[30]G. Weisz, Phys. Rev. **149**, 504 (1966).
[31]F. Bassani and C. P. Parrasvacini, *Electronic States and Optical Properties in Solids* (Pergamon, New York, 1975).
[32]R. A. Faukner, Phys. Rev. **184**, 713 (1965).
[33]W. Kohn, in *Solid State Physics*, edited by F. Seitz and D. Turbull (Academic, New York, 1964), Vol. 5, p. 257.
[34]J. E. Rowe and D. E. Aspnes, Phys. Rev. Lett. **25**, 162 (1970).
[35]R. M. Martin, J. A. Van Vechten, J. E. Rowe, and D. E. Aspnes, Phys. Rev. B **6**, 2500 (1972).